Nanoscale Advances

ROYAL SOCIETY OF CHEMISTRY

PAPER

View Article Online
View Journal | View Issue

Cite this: *Nanoscale Adv.*, 2025, **7**, 310

Enhanced field emission performance of gold nanoparticle decorated Bi_2S_3 nanoflowers†

Gorkshnath H. Gote, [a] Madhura P. Deshpande,[b] Somnath R. Bhopale,[e] Mahendra A. More, *[c] Raphael Longuinhos Monteiro Lobato, [d] Jenaina Ribeiro-Soares [d] and Dattatray J. Late *[d]

Au nanoparticles (NPs) are decorated on hydrothermally synthesized Bi_2S_3 nanorods (NRs) to enhance the field electron emission (FEE) performance as compared to bare Bi_2S_3 nanorods, resulting in reduction in turn-on field from 3.7 to 2.7 V μm^{-1} (at the current density of 1.0 $\mu A\ cm^{-2}$) with significant increment in maximum emission current density from 138 to 604.8 $\mu A\ cm^{-2}$ (at a field of 7.8 V μm^{-1}) respectively. FESEM/TEM reveals that Bi_2S_3 nanoflowers are assembled from Bi_2S_3 NRs of a typical diameter of 120 ± 10 nm, and Au NPs of diameter about 5–10 nm are uniformly decorated onto the surface of NRs to form an Au/Bi_2S_3 composite. XRD analysis suggests that the as-synthesized product consists of orthorhombic Bi_2S_3 NRs decorated with face-centered cubic Au NPs. The XPS spectrum shows the elemental mapping of the as-synthesized Au/Bi_2S_3. Improvement in field emission properties is mainly attributed to a reduction in work function and increasing emitting sites due to Au NP decoration.

Received 2nd July 2024
Accepted 12th November 2024

DOI: 10.1039/d4na00539b

rsc.li/nanoscale-advances

1 Introduction

Field emission is a quantum mechanical tunneling effect in which electrons are emitted from a metal/semiconductor surface into a vacuum under a sufficiently intense electric field. FEE cathodes possess diverse advantages over thermionic emitters with respect to durability, current density, and low energy consumption, which place FEE devices in the competition for next-generation electronics. FEE cathodes are widely used in certain electron-beam devices, such as flat panel displays,[1] scanning electron microscopes,[2] and X-ray sources.[3] The FEE properties of emitters are related to their composition, tip sharpness, conductivity, field enhancement factor, and work function. To increase the field enhancement factor β it is required to reduce tip sizes and modify the work function, by doping, decorating or preparing composites of nanostructured materials. In this sense, much effort has been made to study nanostructure cathodes for FEE applications such as LaB_6 nanowires,[4] carbon nanotubes (CNTs),[1,5] ZnO,[6] TiS nanosheets,[7] as well as composites such as CNTs-LaB_6,[8] rGO-ZnS,[9] rGO-ZnO,[10] Au-ZnO,[11] *etc.* have been reported as possible field emitter materials.

Since the last few years, metal sulfides have been extensively studied due to their tunable optical and electronic properties, so they are extensively used in energy conversion and storage device applications such as solar cells,[12] supercapacitors,[13] Na-ion batteries,[14] *etc.* Among various metal sulfides, Bi_2S_3 is the most extensively researched direct bandgap semiconductor. As shown in Fig. 1b, the Bi_2S_3 crystal structure is formed by the polymerization of the tightly bonded [Bi_4S_6] unit, where each unit is connected by weak Bi–S and S–S interaction.[15] The benefits of low cost, abundance, non-toxicity, and excellent optoelectronic and electrical properties make Bi_2S_3 an excellent material for practical applications, such as in photodetectors,[16] solar cells,[17] photocatalysis,[18,19] supercapacitors,[20] *etc.* Improvement in FEE performance was mainly attempted by increasing the field enhancement factor (depending on the shape/morphology of the emitters) and reducing the work function of nanostructured emitters. In order to improve FEE performance, it is preferred to study composite/heterostructure properties of nanostructured metal sulfides. Recently, number of investigations were made to improve the FEE performance by blending rGO,[21,22] metal oxides,[23,24] sulfides,[25,26] and materials with various metal sulfides of 1D/2D nanostructures. In addition, many efforts have been made to study the morphology-dependent FEE performance of Bi_2S_3 nanostructures.[27–30]

[a]*Sir Parashurambhau College (Autonomous), Department of Physics, Pune-411030, India*

[b]*Department of Chemistry, Research Institute of Chem-Bio Diagnostic Technology, Chung-Ang University, 84 Heukseok-ro, Dongjak District, Seoul 06974, Republic of Korea*

[c]*Centre for Advanced Studies in Materials Science and Condensed Matter Physics, Department of Physics, Savitribai Phule Pune University, Pune-411007, India. E-mail: mam@physics.unipune.ac.in*

[d]*Departamento de Física, Universidade Federal de Lavras, Campus Universitário, PO Box 3037, Lavras, Minas Gerais, 37200-000, Brazil. E-mail: jenaina.soares@ufla.br; datta099@gmail.com*

[e]*School of Physics, IISER Thiruvananthapuram, Thiruvananthapuram, Kerala 695551, India*

† Electronic supplementary information (ESI) available. See DOI: https://doi.org/10.1039/d4na00539b

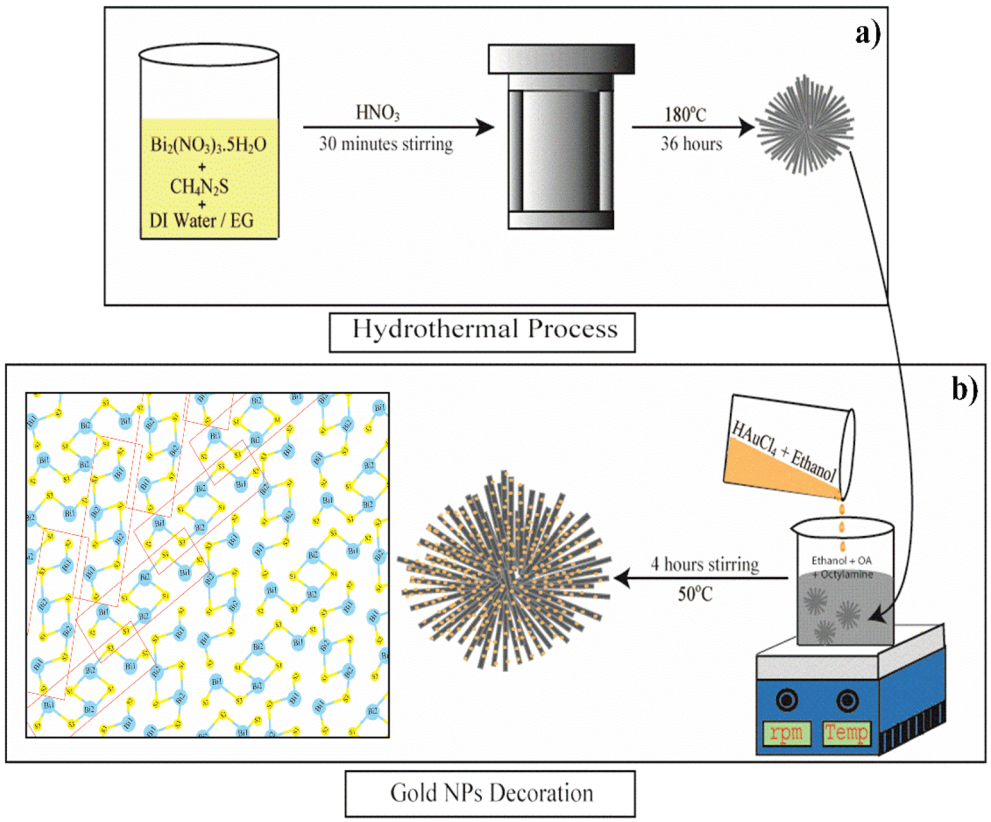

Fig. 1 Schematic depiction of the mechanism of (a) the hydrothermal synthesis of Bi_2S_3 microflowers, (b) Au decoration process on as-synthesized Bi_2S_3 NRs and schematic structure of Bi_2S_3.

However, FEE improvement by work function modulation is less explored for the Bi_2S_3 nanostructure. Our group has investigated the FEE performance of CdS-Bi_2S_3 (ref. 25) and rGO-Bi_2S_3 (ref. 31) composites.

Noble metal NPs (Au, Ag, and Pt) on semiconductors have been extensively studied and exploited in several applications, such as photocatalysis,[32,33] solar cells,[34,35] light-emitting diodes,[36] photodetectors,[37,38] FETs,[39] *etc.* These reports suggest that the decoration of noble metals on nanomaterials enhances the performance of bare nanomaterials due to the Surface Plasmon Resonance (SPR) phenomenon. In the literature survey, it was found that the properties of FEE emitters were greatly influenced by the surface decoration of various morphology nanostructures (ZnO-nanopillars,[11] CdO nanosheets,[40] Si nanowires,[41] SiC nanowires,[42] and graphene sheets[43]) with Au NPs, owing to increase in emitting sites and decrease of the work function. Au metal is well known for its low resistivity, high oxidation resistance, and high structural, electrical and chemical stability. The influence of the decoration of Au NPs on the properties of nanostructures of Bi_2S_3 FEE emitters has not been reported to date.

It has been observed from a literature survey that most nanostructured FEE emitters are decorated with Au NPs by a sputtering process.[11,40–42,44] In this report, we follow a cost-effective and simple chemical method to decorate Au NPs on hydrothermally synthesized Bi_2S_3 NRs to explore the FEE performance. It is observed that the turn-on field of Au/Bi_2S_3 NRs drastically decreased from 3.7 to 2.7 V μm^{-1} at the current density of 1 $\mu A\ cm^{-2}$ and the maximum current density increased from 138 to 604.8 $\mu A\ cm^{-2}$ at an applied field of 7.8 V μm^{-1} as compared to that of pristine Bi_2S_3 NRs. Enhancement in FEE characteristics indicates that metal NP decoration could be an effective route to significantly enhance the FEE performances of the Bi_2S_3 cathodes.

2 Experimental

2.1 Synthesis of Bi_2S_3 nanoflowers

Bismuth sulfide (Bi_2S_3) micro-flowers were synthesised as per the literature report with slight modifications.[45] In a typical synthesis, 2.4 g of bismuth nitrate [$Bi(NO_3)_3 \cdot 5H_2O$] (bismuth precursor) and 0.38 g of thiourea [$CS(NH_2)_2$] (sulfur precursor) were dissolved well into a mixture of 45 ml distilled water and 20 ml ethylene glycol (EG). The resultant solution was subjected to 30 minutes of stirring and 10 minutes of ultra-sonication at room temperature. This yellow homogeneous mixture was then transferred into a Teflon-lined stainless steel autoclave of 80 ml capacity and a few drops of concentrated HNO_3 were added to it. The sealed autoclave was then kept at 180 °C for 36 hours in a muffle furnace. After the reaction, the resulting black precipitate was thoroughly washed (three times) with distilled water and absolute ethanol and collected by centrifugation

(4000 rpm for 10 min). The final product was dried at 60 °C for 24 h in a vacuum. The schematic representation of the Bi_2S_3 microflower synthesis process is shown in Fig. 1a. The resultant black powder was used for further characterization and Au decoration.

2.2 Synthesis of Au/Bi_2S_3 nanostructures

Bi_2S_3 NRs were decorated with Au NPs by following a modified literature report.[46] Briefly, 82 mg of as-synthesized Bi_2S_3 microflowers was dispersed in a 30 ml solvent mixture of 24 ml ethanol, 1.4 ml oleic acid (OA) and 4 ml octylamine. At the same time, 34 mg tetrachloroauric(III) acid ($HAuCl_4 \cdot 3H_2O$) was dispersed into 10 ml of ethanol. Then, the gold precursor solution was added dropwise to the above mixture and stirred for 4 hours at about 50 °C. The grey precipitation was washed several times with ethanol, separated by centrifugation, and then dried overnight in a vacuum. The schematic representation of Au decoration of Bi_2S_3 NRs is shown in Fig. 1b. The collected sample (Au/Bi_2S_3) was used for further characterization and FEE comparison studies with pristine Bi_2S_3.

2.3 Field electron emission measurements

The FEE characteristics of pristine and Au/Bi_2S_3 samples were investigated at room temperature using an in-house developed setup. The distance between emitter sites (cathode) and phosphor screen (anode) is kept at 2 mm, with base pressure being maintained at $\sim 10^{-8}$ mbar during measurements. A high voltage power source (Spellman, U.S.) was used to supply the voltage between two electrodes. The voltage was increased by a step of 20 V and the corresponding increasing current was measured using an electrometer (Keithley 6514) with picoampere sensitivity.

3 Characterization of materials

To examine the crystalline phases of both structures, the X-ray diffraction pattern was obtained by using a Rigaku MicroMax-007 HF with a rotating anode copper X-ray source of wavelength λ Cu K$\alpha = 1.54$ Å which was operated at 40 kV and 30 mA. The morphological and structural characterizations were done using a field emission scanning electron microscope (FESEM, FEI Nova Nano SEM450) and transmission electron microscope. Further structural details and lattice fringe width calculations of both samples were accomplished by high-resolution transmission electron microscopy (HRTEM TEM, JEOL JEM-F200 operated at 200 kV accelerating voltage). X-ray photoelectron spectroscopy was achieved with the use of a near-ambient-pressure X-ray photoelectron spectrometer (XPS, Thermo K-Alpha$^+$ Spectrometer using Al-K$_\alpha$ X-rays, 1486.6 eV) under ultra-high vacuum conditions to study elemental compositions of as-synthesized structures.

4 Results and discussion

4.1 XRD analysis

The phase and crystallinity of samples were studied by the X-ray diffraction technique. Fig. 2a and b show the typical XRD pattern of the as-prepared Au NP decorated Bi_2S_3 and pristine Bi_2S_3 sample respectively. The XRD pattern illustrates that the synthesized sample has an orthorhombic crystal structure with lattice parameters $a = 3.981$ Å, $b = 11.14$ Å, $c = 11.30$ Å (Fig. 2d, JCPDS # 17-0320) which also existed in the Au/Bi_2S_3 sample. The average crystallite size of Bi_2S_3 NRs was found to be $\sim 110 \pm 10$ nm, as calculated using the Debye–Scherer equation. Fig. 2a displays a peak at about $2\theta = 38.10°$, corresponding to the (111) plane of face-centered cubic (fcc) gold, (JCPDS # 04-0784), which gives the evidence for uniform gold decoration. The peak at about $2\theta = 30.50°$ can be attributed to the characteristic peak of BiS_2 (JCPDS #17-0267) indicating the negligible amount of BiS_2 in the as-synthesized samples.

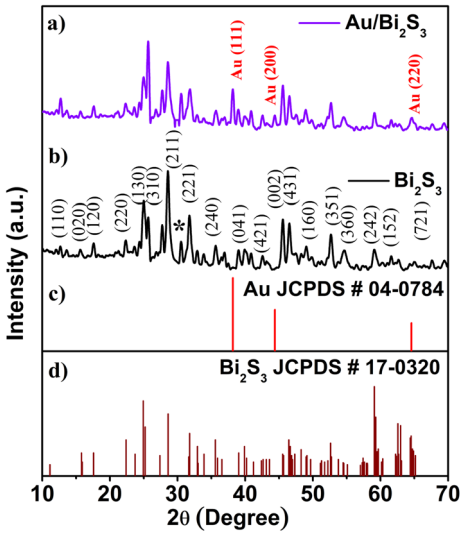

Fig. 2 XRD of the (a) Au/Bi_2S_3 sample and (b) Bi_2S_3; (c) and (d) are JCPDS cards of Au and Bi_2S_3 crystals, respectively.

4.2 FESEM and TEM analysis

FESEM and TEM were used to examine surface morphology, size, and Au particle distribution on the as-prepared sample. Fig. 3a depicts an overview of the sample, where the Bi_2S_3 microflowers are observed with approximately ~4 to 5 μm diameter. Fig. 3b shows typical images assembled from the number of NRs. The inset in Fig. 3b is the high -magnification FESEM image of Bi_2S_3 micro-flowers. It is seen from the TEM image (Fig. 3c) that bare Bi_2S_3 NRs have a smooth surface with length in few microns and about ~120 nm in diameter, which is also endorsed by the average crystallite size calculated from the XRD pattern using the Debye–Scherer equation. The typical enlarged TEM image (Fig. 3d) of the Au decorated Bi_2S_3 nanorods reveals that the Au NPs were uniformly decorated over the entire surface of the Bi_2S_3 NRs without extended agglomerations. The high-resolution TEM (HRTEM) images displayed in Fig. 4a illustrate that the decorated Au NPs have an average diameter of 4–10 nm. The fine HRTEM fringes (Fig. 4b) reveal that the distance between two consecutive planes is 0.239 nm which is identical to the interplanar spacing of face-centered cubic (fcc) Au(111) planes.[47] Fig. 4c and d display the Selected Area

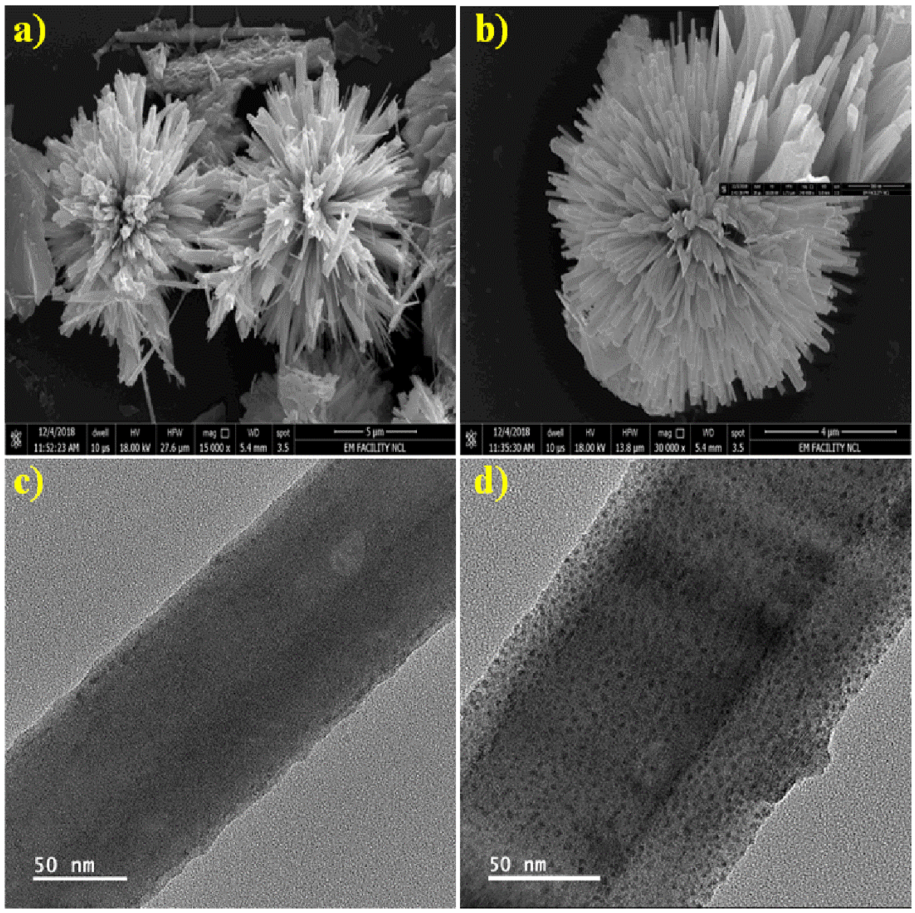

Fig. 3 FESEM images: (a) low magnification Bi_2S_3 microflowers, (b) high magnification Bi_2S_3 with the inset displaying nanorods; TEM images (c and d) of bare Bi_2S_3 and Au decorated Bi_2S_3 NRs, respectively.

Electron Diffraction (SAED) pattern of pristine Bi_2S_3 and Au/Bi_2S_3 NRs.

4.3 XPS analysis

Surface chemical compositions and oxidation states of the as-synthesized product were investigated by XPS analysis. Fig. 5a shows the survey spectra of the sample with and without Au decoration, and gives strong evidence for the existence of Bi and S elements along with the successful decoration of Au on Bi_2S_3. The O and C peaks also arise due to the adsorbed oxygen species on the sample surface, which is commonly observed for samples exposed to the atmosphere and adsorbed carbon species during XPS measurement respectively. Adventitious C1s (284.6 eV) spectra were taken as the reference for calibration. Au $4f_{7/2}$ and $4f_{5/2}$ doublets with binding energies of 83.69 and 87.39 eV are observed in Fig. 5b, which asserts that decorated Au (Au^0 state) is in the metallic form (ref. 48 and 49). As shown in Fig. 5c, the high-resolution spectrum of Bi_{4f} (Bi^{3+} state) shows a doublet at 159.14 ($4f_{7/2}$) and 164.39 eV ($4f_{5/2}$) attributed to spin–orbital coupling separated by 5.31 eV.[49] The binding energy for S2s (S^{2-} state) (Fig. 5d) in the Au/Bi_2S_3 sample is at 224.1 eV which is lower than the binding energy of S2s (S^{2-} state) (225.7 eV) in pristine Bi_2S_3 as per the literature.[49] The Bi and S binding energies are in good agreement with reported values. It is observed that the Au decoration does not severely change the crystallinity of Bi_2S_3 NRs. All XPS plots validate the successful formation of Au/Bi_2S_3.

4.4 Reaction mechanism

In our earlier report, we discussed the synthesis mechanism of Bi_2S_3 microflowers prepared by a simple one-pot hydrothermal method for FEE studies.[31] For the decoration of Au NPs on Bi_2S_3 NRs, $HAuCl_4 \cdot 3H_2O$ was decomposed at 50 °C in an octylamine–oleic acid mixture under ambient conditions. In this reaction, the octylamine–oleic acid mixture acts as both a capping and a reducing agent, which prevents gold NP aggregation and oxidation, as well as makes the particle surface hydrophobic.[50] The polar ethanol solvent was primarily used to dissolve $HAuCl_4 \cdot 3H_2O$. The presence of the hydrocarbon surfactant between gold particles possibly prevents the growth of particles beyond 5–7 nm.[51] To ensure the even mixing of the reactants, the solution was continuously stirred beyond the decoration time and also this ensured the uniform deposition of Au NPs onto the Bi_2S_3 surface as seen in TEM images (Fig. 3d). The pristine Bi_2S_3 and Au/Bi_2S_3 nanocomposites have been fully characterized and their FEE properties studied.

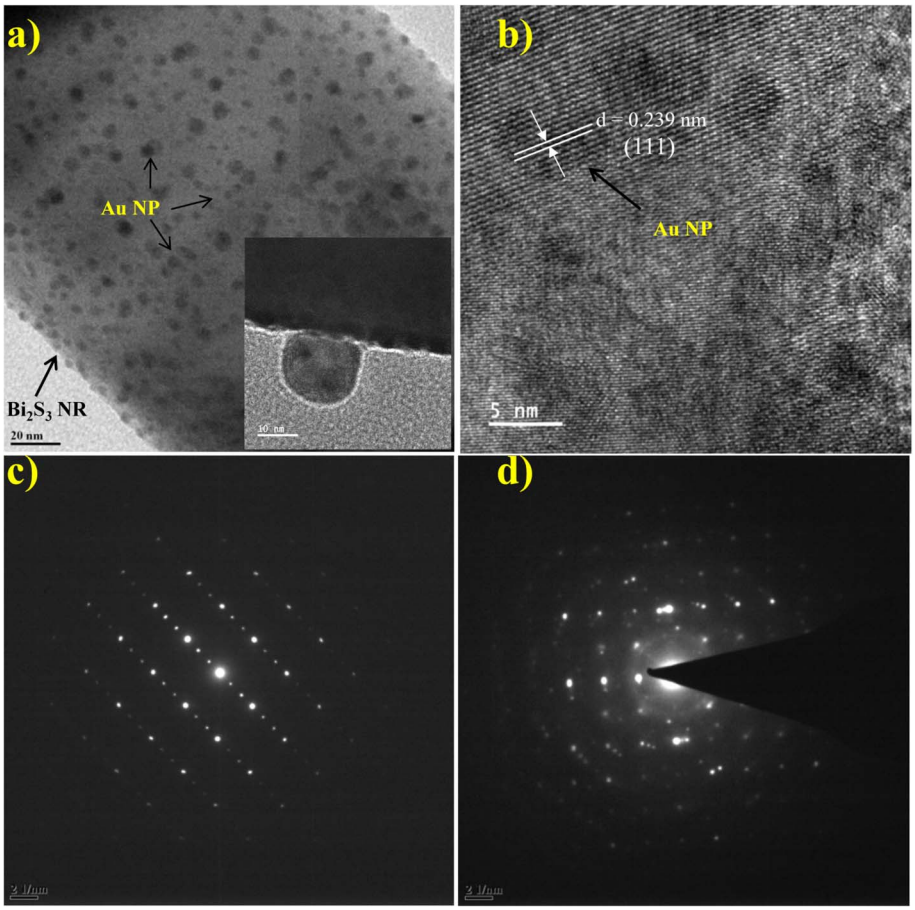

Fig. 4 TEM image of (a) Au/Bi_2S_3 NRs with the inset displaying the NPs; (b) HRTEM image of Au/Bi_2S_3; (c and d) SAED pattern of bare Bi_2S_3 NRs and Au/Bi_2S_3 NRs, respectively.

4.5 Field electron emission (FEE) performance

The dependence of FEE current density over an applied field (J–E) is described by the modified Fowler–Nordheim (F–N) equation:[52]

$$J = \frac{\lambda_m E^2 \beta^2}{\phi} \exp\left(\frac{-b\,\phi^{3/2} v_F}{\beta E}\right) \quad (1)$$

where J is the emission current density, E is the applied average electric field, λ_m is the macroscopic pre-exponential factor ($=1.54 \times 10^{-6}$ A eV V^{-2}), b is a constant ($=6.83$ eV$^{-3/2}$ V nm^{-1}), ϕ is the work function of the emitter, β is the field enhancement factor, and v_F (correction factor) is a particular value of the principal Schottky–Nordheim barrier function v.

Eqn (1) asserts that FEE property enhancement can be achieved by either/both tuning the morphology or/and lowering the work function of the emitter. We have tried to improve the FEE performance of Bi_2S_3 NRs by Au decoration, resulting in reduced work function of Bi_2S_3.

The turn-on and threshold fields, measured from the J–E plot (Fig. 6a), are arbitrarily defined at emission current densities of 1 and 100 μA cm^{-2} respectively. The Au/Bi_2S_3 emitters show the turn-on and threshold fields of 2.7 and 5.2 V μm^{-1} respectively, whereas pristine Bi_2S_3 emitters show the turn-on and threshold fields of 3.7 and 6.8 V μm^{-1} respectively. It is obvious from the results that the FEE properties of pure Bi_2S_3 can be dramatically improved by Au decoration.

A wide range of research groups have reported a significant enhancement in FEE performance due to Au decoration on semiconductor materials.[11,41–44] Zang *et al.*[53] reported that the reduction of Au NP size below 10 nm decreases the work function up to 3.6 eV. In this work, decorated Au NPs have an average size of 4–10 nm, indicating that the work function of Au NPs would be around 3.6 eV, which is less than the work function of Bi_2S_3 NRs (4.93 eV).[25] When Au (metal) and Bi_2S_3 (semiconductor) come into contact, they form a metal–semiconductor junction (Schottky barrier junction). The thermal equilibrium has been achieved through the transfer of electrons from Au (higher) to Bi_2S_3 (lower). The bending of the conduction band (CB) and valence band (VB) in Bi_2S_3 takes place due to the alignment of work functions. This energy band bending reduces the work function of the Bi_2S_3 emitter. Such work function reduction, due to NP decoration of the nanomaterial, shows an improvement of the FEE properties.[54]

The F–N plots (Fig. 6b) derived from the observed (J–E) curves show deviation from the linear nature, in contrast to the expectation of the F–N model. Such discrepancy has been observed in a diverse range of metal–semiconductor

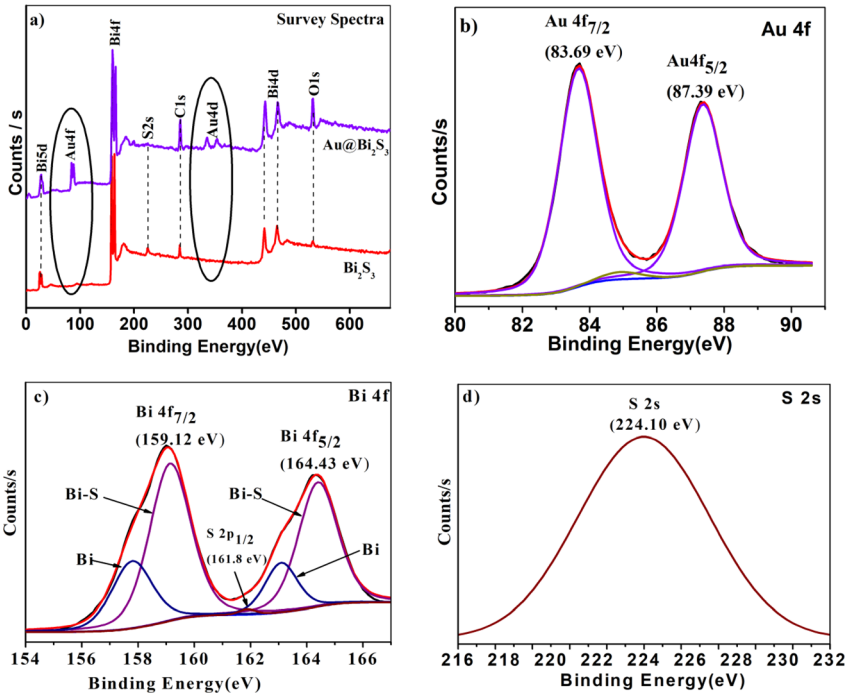

Fig. 5 XPS images of (a) Bi_2S_3 and Au/Bi_2S_3 survey spectra; high resolution spectra of (b) Au^0 state, (c) Bi^{3+} state, (d) S^{2-} state of the Au/Bi_2S_3 sample.

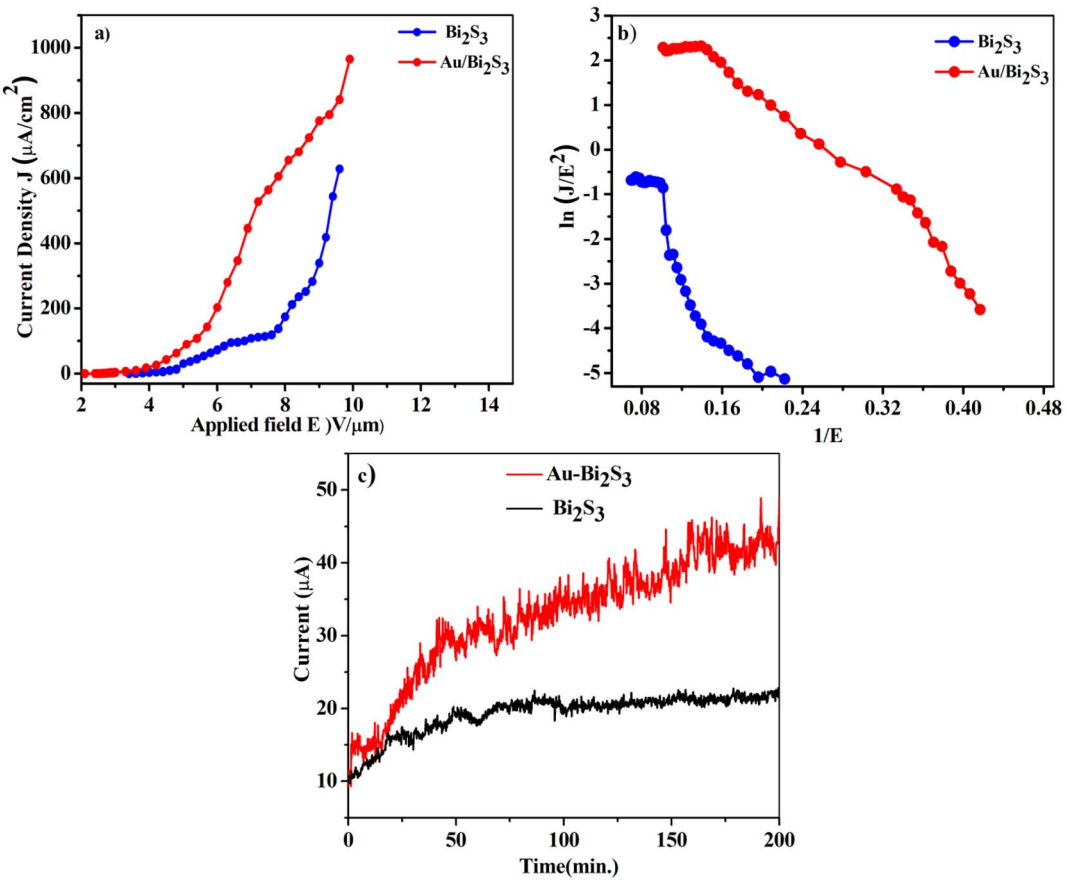

Fig. 6 Plot of field emission current density *versus* applied electric field (*J*–*E*) (a), Fowler–Northeim (F–N) plot (b) of Bi_2S_3 and Au/Bi_2S_3, respectively. (c) Field emission current stability plots at 10 μA.

Table 1 FEE characteristic parameters of various semiconducting planar emitters

Sr. no.	Emitter details	Morphology	Turn-on field or voltage	Reference
1	MoS_2	Nanoflowers	12 V μm^{-1}	55
2	CNTs	Nanotubes	50 to 100 V	56 and 57
3	Au/ZnO	Nanowires	6.2 V μm^{-1}	58
4	AuBN	Nanocomposites	3.9 V μm^{-1} at 10 nA cm^{-2}	59
5	Au/graphene	Nanosheets	3.84 V μm^{-1}	60
6	Au/TiO_2	Nanotubes	2.8 V μm^{-1} at 10 μA cm^{-2}	61
7	Au/Bi_2S_3	Micro-flowers	2.7 V μm^{-1} at 1 μA cm^{-2}	Present work

composites. This discrepancy can be supported by emission from the lower edge of the CB being dominant at a low field. On the other hand, at a high field, the emission current also contributes to the electrons in the upper edge of the CB.[62] It is observed that the nonlinearity of the F–N plot diminishes in the Au/Bi_2S_3 emitter, indicating a more metallic behavior of the emitter. Furthermore, a careful observation reveals 'flattening' of the F–N plots in the high field region. For planar emitters, most of the researchers have noticed a 'non-linear' nature of the F–N plots, along with the tendency to show 'flattening' in the high field region, which had been attributed to various effects like the field screening effect, field penetration and band bending (for semiconducting emitters), *etc.* However, one of the root causes of such discrepancy is failure of the fundamental F–N model. It has been realized that the effect and/or contribution due to space charge limited currents has been ignored. Various researchers have focused their studies towards amending the fundamental F–N equation so as to justify the FEE behaviour of planar emitters. Herein, a planar emitter is referred to as an assembly of nanostructures deposited in a thin film form on suitable substrates. In tune with the advancement in planar emitter based electron sources and new devices, these alterations are important in providing better formulations for simulations.

In this context, Richard Forbes has put in significant and consistent efforts towards modification of the fundamental F–N model.[52,63,64] In tune with these efforts, Zhang *et al.* have presented an overview of the fundamental physics of space–charge interactions in various media addressing the critical developments on various theoretical aspects of the space–charge limited current (SCLC) model, its physics at the nanoscale, and transitions between electron emission mechanisms and material properties.[65] Very recently, in order to corroborate the advancements in utilization of electron sources, particularly simulations of the devices, Kevin Jensen has provided useful formulations considering the effect of "space–charge" (commonly described by the Child–Langmuir law) so as to guarantee correct numerical evaluation of the fundamental equations describing the various electron emission models.[66]

Furthermore, to showcase the technological importance of the observed FEE parameters, an attempt is made to compare the values of turn-on and threshold fields along with maximum emission current density extracted from similar emitters, Table1.

Finally, to test the quality of the as-synthesized Au/Bi_2S_3 emitters in comparison with pristine Bi_2S_3, we have investigated the long-term current stability (*I*–*t*) plot. The stability of the emitters has been observed for more than 3 h corresponding to a current density of 10 μA cm^{-2}. It is observed that fluctuations in current density for the Au/Bi_2S_3 emitter (the standard deviation of ~3.86%) are somewhat more than for the bare Bi_2S_3 (the standard deviation of about ~2.07%), possibly due to increase in emitting sites for the Au/Bi_2S_3 emitter. The fluctuation in electron emission current can be attributed to the adsorption/desorption and bombardments of ions/atoms on the emitter surface.[67,68] The smoothness in the current stability (*I*–*t*) plot of the Au/Bi_2S_3 sample is also attributed to the protection of Bi_2S_3 NR emitters from ion/atom bombardments during the FEE mechanism due to the good chemical stability of Au NPs. The emitter also reveals good repeatability of results by testing the same samples several times.

5 Conclusions

In summary, we have reported the synthesis of Bi_2S_3 emitters with 120 ± 10 nm diameter, *via* a simple hydrothermal route followed by the uniform decoration of Au NPs with size ~4–10 nm. FEE results show that the turn-on field of the Au/Bi_2S_3 emitter reduced from 3.7 to 2.7 V μm^{-1} at 1.0 μA cm^{-2} and the maximum current density increased from 138 to 604 μA cm^{-2} at field 7.8 V μm^{-1} as compared to that of pristine Bi_2S_3. The improved FEE performance of Au/Bi_2S_3 is attributed to the lowering of the work function of pristine Bi_2S_3 and increasing emission sites due to Au NP decoration. Therefore, Au decoration on Bi_2S_3 was achieved by a simple and cost-effective chemical method compared to the sputtering process. The Au decorated FEE emitters can be used as a potential candidate for flexible flat panel displays, efficient electron guns, and e-paper applications.

Data availability

All data generated or analyzed during this study are included in this published article and its ESI.†

Author contributions

GG and MD performed the synthesis experiments, characterization, and analysis. FEE analysis was done by SB and MM. GG

wrote the first draft of the paper. GG, DL, and MM revised the writing of the manuscript and data calculations. RLML and J. Ribeiro-Soares in the revised the writing of the manuscript and data calculations. DL guided the research and conceived the final project.

Conflicts of interest

The authors declare no conflicts of interest.

Acknowledgements

This work was financially supported by the SPPU Research Foundation research grant. DJL thanks Foundation for Research of the State of Minas Gerais (UFLA, Brazil) - FAPEMIG (Project Grant No. APQ-04229-23) for funding. GG thanks Rashtriya Uchchatar Shiksha Abhiyan (RUSA) for research funding.

References

1 W. Choi, D. Chung, J. Kang, H. Kim, Y. Jin, I. Han, Y. Lee, J. Jung, N. Lee and G. Park, Fully sealed, high-brightness carbon-nanotube field-emission display, *Appl. Phys. Lett.*, 1999, **75**(20), 3129–3131.

2 A. V. Crewe, M. Isaacson and D. Johnson, A simple scanning electron microscope, *Rev. Sci. Instrum.*, 1969, **40**(2), 241–246.

3 F. Baker, A. Osborn and J. Williams, Field emission from carbon fibres: a new electron source, *Nature*, 1972, **239**(5367), 96.

4 H. Zhang, J. Tang, Q. Zhang, G. Zhao, G. Yang, J. Zhang, O. Zhou and L. C. Qin, Field emission of electrons from single LaB6 nanowires, *Adv. Mater.*, 2006, **18**(1), 87–91.

5 S. Fan, M. G. Chapline, N. R. Franklin, T. W. Tombler, A. M. Cassell and H. Dai, Self-oriented regular arrays of carbon nanotubes and their field emission properties, *Science*, 1999, **283**(5401), 512–514.

6 C. J. Lee, T. Lee, S. Lyu, Y. Zhang, H. Ruh and H. Lee, Field emission from well-aligned zinc oxide nanowires grown at low temperature, *Appl. Phys. Lett.*, 2002, **81**(19), 3648–3650.

7 A. S. Pawbake, R. T. Khare, J. O. Island, E. Flores, J. R. Ares, C. Sanchez, I. J. Ferrer, M. Pawar, O. Frank and M. A. More, Titanium Trisulfide Nanosheets and Nanoribbons for Field Emission-Based Nanodevices, *ACS Appl. Nano Mater.*, 2023, **6**(1), 44–49.

8 R. Patra, S. Ghosh, E. Sheremet, M. Jha, R. Rodriguez, D. Lehmann, A. Ganguli, H. Schmidt, S. Schulze and M. Hietschold, Enhanced field emission from lanthanum hexaboride coated multiwalled carbon nanotubes: correlation with physical properties, *J. Appl. Phys.*, 2014, **116**(16), 164309.

9 S. R. Bansode, M. A. More and R. B. Sharma, ZnS–RGO nanocomposite structures: synthesis, characterization and field emission properties, *New J. Chem.*, 2023, **47**(5), 2273–2278.

10 W. T. Zheng, Y. M. Ho, H. W. Tian, M. Wen, J. L. Qi and Y. A. Li, Field emission from a composite of graphene sheets and ZnO nanowires, *J. Phys. Chem. C*, 2009, **113**(21), 9164–9168.

11 Y.-M. Chang, M.-L. Lin, T.-Y. Lai, H.-Y. Lee, C.-M. Lin, Y.-C. S. Wu and J.-Y. Juang, Field Emission Properties of Gold Nanoparticle-Decorated ZnO Nanopillars, *ACS Appl. Mater. Interfaces*, 2012, **4**(12), 6676–6682.

12 X. Yu, J. Zhu, Y. Zhang, J. Weng, L. Hu and S. Dai, $SnSe_2$ quantum dot sensitized solar cells prepared employing molecular metal chalcogenide as precursors, *Chem. Commun.*, 2012, **48**(27), 3324–3326.

13 M. Acerce, D. Voiry and M. Chhowalla, Metallic 1T phase MoS_2 nanosheets as supercapacitor electrode materials, *Nat. Nanotechnol.*, 2015, **10**(4), 313.

14 K. Zhang, Z. Hu, X. Liu, Z. Tao and J. Chen, $FeSe_2$ microspheres as a high performance anode material for Na ion batteries, *Adv. Mater.*, 2015, **27**(21), 3305–3309.

15 R. Caracas and X. Gonze, First-principles study of the electronic properties of A2B3 minerals, with A = Bi,Sb and B = S,Se, *Phys. Chem. Miner.*, 2005, **32**(4), 295–300.

16 G. Chen, Y. Yu, K. Zheng, T. Ding, W. Wang, Y. Jiang and Q. Yang, Fabrication of Ultrathin Bi_2S_3 Nanosheets for High Performance, Flexible, Visible–NIR Photodetectors, *Small*, 2015, **11**(24), 2848–2855.

17 B. Xu, G. Wang and H. Fu, Enhanced photoelectric conversion efficiency of dye-sensitized solar cells by the incorporation of flower-like Bi_2S_3:Eu^{3+} sub-microspheres, *Sci. Rep.*, 2016, **6**, 23395.

18 A. Sarkar, A. B. Ghosh, N. Saha, A. K. Dutta, D. N. Srivastava, P. Paul and B. Adhikary, Enhanced photocatalytic activity of Eu-doped Bi_2 S_3 nanoflowers for degradation of organic pollutants under visible light illumination, *Catal. Sci. Technol.*, 2015, **5**(8), 4055–4063.

19 J. Zhou, G. Tian, Y. Chen, Y. Shi, C. Tian, K. Pan and H. Fu, ERRATUM: Growth rate controlled synthesis of hierarchical Bi_2S_3/In_2S_3 core/shell microspheres with enhanced photocatalytic activity, *Sci. Rep.*, 2014, **4**, 4027.

20 S. P. Vattikuti, A. K. R. Police, J. Shim and C. Byon, Sacrificial-template-free synthesis of core–shell C@Bi_2 S_3 heterostructures for efficient supercapacitor and H_2 production applications, *Sci. Rep.*, 2018, **8**(1), 4194.

21 C. S. Rout, P. D. Joshi, R. V. Kashid, D. S. Joag, M. A. More, A. J. Simbeck, M. Washington, S. K. Nayak and D. J. Late, Enhanced field emission properties of doped graphene nanosheets with layered SnS_2, *Appl. Phys. Lett.*, 2014, **105**(4), 043109.

22 C. S. Rout, P. D. Joshi, R. V. Kashid, D. S. Joag, M. A. More, A. J. Simbeck, M. Washington, S. K. Nayak and D. J. Late, Superior field emission properties of layered WS_2-RGO nanocomposites, *Sci. Rep.*, 2013, **3**, 3282.

23 C. Song, K. Yu, H. Yin, H. Fu, Z. Zhang, N. Zhang and Z. Zhu, Highly efficient field emission properties of a novel layered VS_2/ZnO nanocomposite and flexible VS_2 nanosheet, *J. Mater. Chem. C*, 2014, **2**(21), 4196–4202.

24 J. Li, K. Yu, Y. Tan, H. Fu, Q. Zhang, W. Cong, C. Song, H. Yin and Z. Zhu, Facile synthesis of novel MoS_2@SnO_2 hetero-nanoflowers and enhanced photocatalysis and field-

emission properties, *Dalton Trans.*, 2014, **43**(34), 13136–13144.

25 P. K. Bankar, M. S. Pawar, A. S. Pawbake, S. S. Warule, D. J. Late and M. A. More, Spatially branched CdS–Bi_2 S_3 heteroarchitecture: single step hydrothermal synthesis approach with enhanced field emission performance and highly responsive broadband photodetection, *RSC Adv.*, 2016, **6**(97), 95092–95100.

26 S. R. Bansode, K. V. Harpale, P. Mutadak, K. M. Sonawane, M. G. Chaskar, M. A. More and R. B. Sharma, Morphology-dependent field emission investigations from the 2-dimensional Bi_2Se_3-RGO nanocomposites, *Mater. Sci. Eng., B*, 2021, **274**, 115450.

27 X. Yu and C. Cao, Photoresponse and field-emission properties of bismuth sulfide nanoflowers, *Cryst. Growth Des.*, 2008, **8**(11), 3951–3955.

28 Y. Yu, C. Jin, R. Wang, Q. Chen and L.-M. Peng, High-quality ultralong Bi_2S_3 nanowires: structure, growth, and properties, *J. Phys. Chem. B*, 2005, **109**(40), 18772–18776.

29 S. S. Warule, R. Kashid, D. Shinde, N. S. Chaudhari, B. Kale and M. More, Architectured Bi_2S_3 nanoflowers: photoenhanced field emission study, 2012, **14**.

30 Y. Li, S. Nambiar, Y. Sun, C. N. R. Rao and J. T. W. Yeow, In Experimental study on field emission performance of bismuth sulfide nanoflowers, *14th IEEE International Conference on Nanotechnology*, 2014, pp. 1–4.

31 G. H. Gote, S. R. Bhopale, M. A. More and D. J. Late, Realization of Efficient Field Emitter Based on rGO-Bi_2S_3 Heterostructures, *Phys. Status Solidi A*, 2019, **216**(18), 1900121.

32 P. Wang, B. Huang, X. Zhang, X. Qin, H. Jin, Y. Dai, Z. Wang, J. Wei, J. Zhan and S. Wang, Highly efficient visible light plasmonic photocatalyst Ag@AgBr, *Chem.–Eur. J.*, 2009, **15**(8), 1821–1824.

33 Y. Tian and T. Tatsuma, Mechanisms and applications of plasmon-induced charge separation at TiO_2 films loaded with gold nanoparticles, *J. Am. Chem. Soc.*, 2005, **127**(20), 7632–7637.

34 L.-B. Luo, C. Xie, X.-H. Wang, Y.-Q. Yu, C.-Y. Wu, H. Hu, K.-Y. Zhou, X.-W. Zhang and J.-S. Jie, Surface plasmon resonance enhanced highly efficient planar silicon solar cell, *Nano Energy*, 2014, **9**, 112–120.

35 V. E. Ferry, J. N. Munday and H. A. Atwater, Design considerations for plasmonic photovoltaics, *Adv. Mater.*, 2010, **22**(43), 4794–4808.

36 K. Okamoto, I. Niki, A. Shvartser, Y. Narukawa, T. Mukai and A. Scherer, Surface-plasmon-enhanced light emitters based on InGaN quantum wells, *Nat. Mater.*, 2004, **3**(9), 601.

37 L.-B. Luo, L.-H. Zeng, C. Xie, Y.-Q. Yu, F.-X. Liang, C.-Y. Wu, L. Wang and J.-G. Hu, Light trapping and surface plasmon enhanced high-performance NIR photodetector, *Sci. Rep.*, 2014, **4**, 3914.

38 C.-C. Chang, Y. D. Sharma, Y.-S. Kim, J. A. Bur, R. V. Shenoi, S. Krishna, D. Huang and S.-Y. Lin, A surface plasmon enhanced infrared photodetector based on InAs quantum dots, *Nano Lett.*, 2010, **10**(5), 1704–1709.

39 J. Lin, H. Li, H. Zhang and W. Chen, Plasmonic enhancement of photocurrent in MoS_2 field-effect-transistor, *Appl. Phys. Lett.*, 2013, **102**(20), 203109.

40 V. S. Bagal, G. P. Patil, A. B. Deore, S. R. Suryawanshi, D. J. Late, M. A. More and P. G. Chavan, Surface modification of aligned CdO nanosheets and their enhanced field emission properties, *RSC Adv.*, 2016, **6**(47), 41261–41267.

41 F. Zhao, G.-a. Cheng, R.-t. Zheng, D.-d. Zhao, S.-l. Wu and J.-h. Deng, Field emission enhancement of Au–Si nanoparticle-decorated silicon nanowires, *Nanoscale Res. Lett.*, 2011, **6**(1), 176.

42 Q. Chen, S. Chen, F. Gao, L. Wang, Z. Xie and W. Yang, Enhanced field emission of Au nanoparticle-decorated SiC nanowires, *J. Mater. Chem. C*, 2016, **4**(7), 1363–1368.

43 L. Chen, H. He, D. Lei, Q. Menggen, L. Hu and D. Yang, Field emission performance enhancement of Au nanoparticles doped graphene emitters, *Appl. Phys. Lett.*, 2013, **103**(23), 233105.

44 H. Chen, H. Zhang, L. Fu, Y. Chen, J. S. Williams, C. Yu and D. Yu, Nano Au-decorated boron nitride nanotubes: Conductance modification and field-emission enhancement, *Appl. Phys. Lett.*, 2008, **92**(24), 243105.

45 Y. Tian, T.-t. Ding, X.-l. Zhu, Y.-f. Tu and G. Zheng, Bi_2S_3 microflowers assembled from one-dimensional nanorods with a high photoresponse, *J. Mater. Sci.*, 2015, **50**(16), 5443–5449.

46 J. L. Chen, V. Nalla, G. Kannaiyan, V. Mamidala, W. Ji and J. J. Vittal, Synthesis and nonlinear optical switching of Bi2S3 nanorods and enhancement in the NLO response of Bi2S3@Au nanorod-composites, *New J. Chem.*, 2014, **38**(3), 985–992.

47 X. Huang, S. Li, Y. Huang, S. Wu, X. Zhou, S. Li, C. L. Gan, F. Boey, C. A. Mirkin and H. Zhang, Synthesis of hexagonal close-packed gold nanostructures, *Nat. Commun.*, 2011, **2**, 292.

48 J. Luo, Y. Liu, Y. Niu, Q. Jiang, R. Huang, B. Zhang and D. Su, Insight into the chemical adsorption properties of CO molecules supported on Au or Cu and hybridized Au–CuO nanoparticles, *Nanoscale*, 2017, **9**(39), 15033–15043.

49 S. K. Saha and A. J. Pal, Schottky diodes between Bi2S3 nanorods and metal nanoparticles in a polymer matrix as hybrid bulk-heterojunction solar cells, *J. Appl. Phys.*, 2015, **118**(1), 014503.

50 P. d. l. Presa, M. Multigner, J. d. l. Venta, M. A. García and M. L. Ruiz-González, Structural and magnetic characterization of oleic acid and oleylamine-capped gold nanoparticles, *J. Appl. Phys.*, 2006, **100**(12), 123915.

51 Y. Min, M. Akbulut, K. Kristiansen, Y. Golan and J. Israelachvili, The role of interparticle and external forces in nanoparticle assembly, in *Nanoscience and Technology: A Collection of Reviews from Nature Journals*, World Scientific, 2010, pp. 38–49.

52 R. G. Forbes, Extraction of emission parameters for large-area field emitters, using a technically complete Fowler–Nordheim-type equation, *Nanotechnology*, 2012, **23**(9), 09570.

53 Y. Zhang, O. Pluchery, L. Caillard, A.-F. Lamic-Humblot, S. Casale, Y. J. Chabal and M. Salmeron, Sensing the Charge State of Single Gold Nanoparticles *via* Work Function Measurements, *Nano Lett.*, 2015, **15**(1), 51–55.

54 C. Ye, Y. Bando, X. Fang, G. Shen and D. Golberg, Enhanced field emission performance of ZnO nanorods by two alternative approaches, *J. Phys. Chem. C*, 2007, **111**(34), 12673–12676.

55 F. Giubileo, A. Grillo, M. Passacantando, F. Urban, L. Iemmo, G. Luongo and A. Di Bartolomeo, Field emission characterization of MoS_2 nanoflowers, *Nanomaterials*, 2019, **9**(5), 717.

56 F. Giubileo, A. Di Bartolomeo, L. Iemmo, G. Luongo and F. Urban, Field emission from carbon nanostructures, *Appl. Sci.*, 2018, **8**(4), 526.

57 S. B. Fairchild, T. A. de Assis, J. H. Park, M. Cahay, J. Bulmer, D. E. Tsentalovich and M. Pasquali, Strongly anisotropic field emission from highly aligned carbon nanotube films, *J. Appl. Phys.*, 2021, **129**(12), 125103.

58 K. Zheng, Z. Zhang, X. Li, J. She, S. Deng, N. Xu and J. Chen, Field emission from Au nanoparticles decorated ZnO nanowires, in *2018 31st International Vacuum Nanoelectronics Conference (IVNC)*, IEEE, 2018, pp. 1–2.

59 H. Chen, H. Zhang, L. Fu, Y. Chen, J. S. Williams, C. Yu and D. Yu, Nano Au-decorated boron nitride nanotubes: Conductance modification and field-emission enhancement, *Appl. Phys. Lett.*, 2008, **92**(24), 243105.

60 J. Xu, Q. Wang, Z. Tao, Z. Qi, Y. Zhai, W. Lei and X. Zhang, Enhanced electron emission of directly transferred few-layer graphene decorated with gold nanoparticles, *RSC Adv.*, 2016, **6**(81), 78170–78175.

61 G. P. Patil, V. S. Bagal, S. R. Suryawanshi, D. J. Late, M. A. More and P. G. Chavan, Observation of enhanced field emission properties of Au/TiO_2 nanocomposite, *Appl. Phys. A: Mater. Sci. Process.*, 2016, **122**, 1–11.

62 A. A. Al-Tabbakh, M. A. More, D. S. Joag, I. S. Mulla and V. K. Pillai, The Fowler–Nordheim plot behavior and mechanism of field electron emission from ZnO tetrapod structures, *ACS Nano*, 2010, **4**(10), 5585–5590.

63 R. G. Forbes, The theoretical link between voltage loss, reduction in field enhancement factor, and Fowler–Nordheim-plot saturation, *Appl. Phys. Lett.*, 2017, **110**(13), 133109.

64 T. A. de Assis, F. F. Dall'Agnol and R. G. Forbes, Field emitter electrostatics: a review with special emphasis on modern high-precision finite-element modelling, *J. Phys.: Condens. Matter*, 2022, **34**(49), 493001.

65 P. Zhang, Y. S. Ang, A. L. Garner, Á. Valfells, J. W. Luginsland and L. K. Ang, Space–charge limited current in nanodiodes: ballistic, collisional, and dynamical effects, *J. Appl. Phys.*, 2021, **129**(10), 100902.

66 K. L. Jensen, Tutorial: the equations of electron emission and their evaluation, *J. Appl. Phys.*, 2024, **135**(11), 111101.

67 C. Kleint, Surface diffusion model of adsorption-induced field emission flicker noise: I. Theory, *Surf. Sci.*, 1971, **25**(2), 394–410.

68 H. Todokoro, N. Saitou and S. Yamamoto, Role of ion bombardment in field emission current instability, *Jpn. J. Appl. Phys.*, 1982, **21**(10R), 1513.